Proceedings of the ASME 2015 International Technical Conference and Exhibition on Packaging and Integration of Electronic and Photonic Microsystems and ASME 2015 13th International Conference on Nanochannels, Microchnnels, and Minichannels InterPACKICNMM2015 July 6-9, 2015, San Francisco, California, USA

InterPACKICNMM2015-48459

THERMAL STABILITY OF RARE EARTH OXIDE COATED SUPERHYDROPHOBIC MICROSTRUCTURED METALLIC SURFACES

Anton Hassebrook
University of Nebraska-Lincoln
Department of Mechanical and Materials Engineering
Lincoln, NE, USA

Michael J. Lucis
University of Nebraska-Lincoln
Department of Mechanical and Materials Engineering
Nebraska Center for Materials and Nanoscience (NCMN)
Lincoln, NE, USA

Jeffrey E. Shield
University of Nebraska-Lincoln
Department of Mechanical and Materials Engineering
Nebraska Center for Materials and Nanoscience (NCMN)
Lincoln, NE, USA

Craig Zuhlke
University of Nebraska-Lincoln
Department of Electrical and Computer Engineering
Lincoln, NE, USA

Troy Anderson
University of Nebraska-Lincoln
Department of Electrical and Computer Engineering
Lincoln, NE, USA

Dennis Alexander
University of Nebraska-Lincoln
Department of Electrical and Computer Engineering
Lincoln, NE, USA

George Gogos
University of Nebraska-Lincoln
Department of Mechanical and Materials Engineering
Lincoln, NE, USA

Sidy Ndao
University of Nebraska-Lincoln
Department of Mechanical and Materials Engineering
Lincoln, NE, USA
sndao2@unl.edu

ABSTRACT

In this paper, we present a method of generating nearly superhydrophobic surfaces from Femtosecond Laser Surface Processed (FLSP) metallic substrates and the study of their thermal stability at high temperatures. Using an FLSP process, hierarchical micro/nano structures were fabricated on stainless steel 316 after which a 200 nm Cerium Oxide (CeO_2) film was sputtered onto the surface. Before CeO_2 deposition, the contact angle of sample was measured. Post CeO_2 deposition, the contact angles were measured again. As a result of the cerium oxide deposition, the contact angle of the originally hydrophilic FLSP surface turned near superhydrophobic with an equilibrium contact angle of approximately 140°. Subsequently, the coated surfaces were annealed in air. The surface maintained its high contact angle from room temperature to about 160°C, after which it lost its hydrophobicity due to hydrocarbon burn off. For each annealing temperature, we monitored the chemical composition for the cerium oxide-coated FLSP surface using energy dispersive x-ray spectroscopy (EDS) and X-ray diffraction (XRD). Under a nitrogen rich annealing environment, the nearly superhydrophobic FLSP metallic surface maintained its high contact angle up to temperatures as high as 350°C. To further understand the physics behind the observed phenomenon, we investigated two additional samples of polished stainless steel 310 again coated with 200 nm of CeO_2.

INTRODUCTION

Condensation of water vapor is one of the most important natural phenomena used by humans today. A large number of industrial processes such as power generation and refrigeration depend on condensation for operation. Typically, industrial condensers are made from metals such as copper, aluminum, and stainless steel; however, these metals, and their native oxides have very high surface energies resulting in spreading of condensate across the condenser surface. Due to this wetting effect, condensate forms a film (filmwise condensation) which blankets the surface thereby imposing an additional thermal resistance. Conversely, materials that have low surface energy repel water allowing condensate to form and shed as individual drops; this allows for more effective heat transfer between the surface and the vapor. However, materials with low surface energy tend to be nonconductive, which increases the overall thermal resistance of the system, often times erasing any benefit gained from dropwise condensation. It is therefore desirable to create a metallic surface that is superhydrophobic (contact angle >150˚) with low roll off angle (<5˚). To create a superhydrophobic surface on metals, which have a relatively high surface energy, either high surface area structures made of a low surface energy material must be fabricated on the metal surface or the metal must be micro/nanostructured and then coated with a low surface energy material. Several different types of materials have shown promise as hydrophobic coatings including self-assembled monolayers, polymeric materials, noble metals, and rare earth oxides (REO) [1]. It has also been shown that hydrophilic materials can be made superhydrophobic through the use of "doubly reentrant structures" [2,3].

Recently, silanization of surfaces has attracted attention with several researchers [4–6] showing promising results with silane based coatings. These coatings can be made very thin in order to limit thermal resistance while maintaining superhydrophobic nature. This method, however, has not proven to be durable and is therefore not optimal for industrial purposes [7]. To combat durability issues researchers have developed "self-healing" coatings [8,9]. These coatings are based on fluoroalkylsilane which can migrate across a surface to refunctionalize degraded areas. In the case of [8], damaged surfaces with superhydrophilic properties were left in humid air for 4 hours, after which superhydrophobic properties were completely regained. In the case of [9], samples only needed to be heated to 135˚C for 3 minutes to restore superhydrophobicity. Furthermore, their coating showed robust behavior with superhydrophobic properties persisting for 100 cycles.

Polymer coatings [10,11] share many of the features gained from silane coatings such as excellent hydrophobic properties achievable with very low coating thicknesses. However, they also have the same challenges, namely a compromise between coating thickness, thermal resistance, and durability. Paxson et. al. [7] used Initiated Chemical Vapor Deposition (iCVD) to create a poly-(perfluorodecyl acrylate)-co-divinyl benzene (p(PFDA-co-DVB)) grafted polymer coating which maintained dropwise condensation in an accelerated endurance test for 48 hours. They compared their results to a siloxane based coating which degenerated to filmwise condensation in only 30 minutes.

Noble metals have also been used to create hydrophobic coatings [12–14], and have shown sustained dropwise condensation. However, these materials are intrinsically hydrophilic, and thus depend on surface contamination such as hydrocarbons in the ambient air that adsorb onto the surface of the metals in order to reduce their surface energy. One particular study reported a gold surface maintaining dropwise condensation for up to five years in a closed environment [12]; however, gold and other noble metals are far too expensive for this approach to be economically feasible.

One recently reported method for decreasing surface energy of a metallic substrate used ceramic coating made up of the intrinsically hydrophobic lanthanide series oxides [15]. The authors attributed the hydrophobicity of these rare earth oxide ceramics to their unique electron structure, arguing that "the unfilled 4f orbitals are shielded from interactions with the surrounding environment by the full octet of electrons in the $5s^2p^6$ outer shell". Contact angle measurements showed hydrophobic behavior with measured angles ranging from 100˚ to 110˚; additionally, surfaces coated with these ceramics exhibited dropwise condensation. It was noted however, that when the ceramic coatings were placed in a high temperature, abrasive environment, that hydrophobic properties were lost. This was attributed to destruction of the fragile surface features and delamination of the ceramic coating. In another study [16], it was found that lanthanide series ceramics are not intrinsically hydrophobic as previously thought, but rather adsorb hydrocarbons from ambient air in order to minimize their free surface energy. By monitoring carbon content in relation to contact angle, it was shown that perfectly clean REO surfaces are superhydrophilic (contact angle ~ 0˚), with contact angle increasing proportionally to surface carbon content. While REO surfaces are dependent upon hydrocarbon contamination in the same matter as the previously discussed noble metal coatings, the authors did note some advantages over the currently used technology. When compared to polymer coatings, REO's have significantly increased thermal conductivity. This allows for much thicker coatings to be applied without significant increase to thermal resistance, which could help to combat durability issues like delamination. Furthermore, when compared to noble metals, REO's are very cheap, so integrating them with current facilities would have a significantly decreased initial investment.

Consequentially, REO's show much promise as coating materials for condensers; however, studies on their heat transfer performance and durability are nonexistent. Therefore, the purpose of this work was to evaluate the thermal stability of hydrophobic and superhydrophobic REO coatings on stainless steel. This was accomplished by monitoring the contact angle of a flat mirror-polished and micro/nanoscale roughened test surface while they underwent cyclic heat treatments.

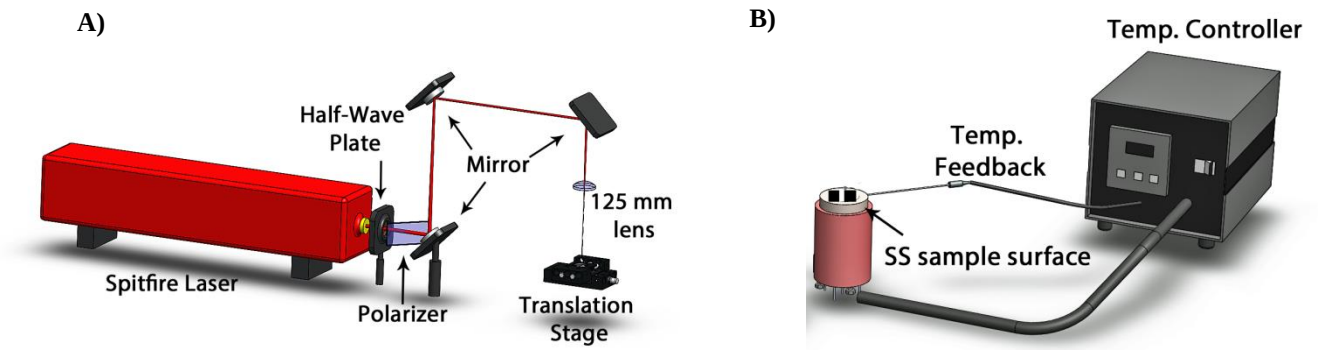

Figure 1. (A) Femtosecond laser surface processing setup. (B) Test surface heating block setup.

EXPERIMENTAL PROCEDURES

Heat treatment experiments were first carried out on a processed microstructured surface due to the possibility of increased hydrocarbon adsorption [17]; the processed sample underwent Femtosecond Laser Surface Processing (FLSP), while another was polished to a mirror-finish for control. FLSP creates a quasi-periodic, self-organized, hierarchical surface with micron scale conical structures coated in a fine layer of nanoparticles [18–23]. This dual scale roughness causes the surface to become superhydrophilic when clean; however, when covered with a low surface energy material, it allows the surface to become superhydrophobic with low contact angle hysteresis due to the Cassie-Baxter effect [24].

FLSP generates multiscale surface structures by inducing a complex combination of multiple self-organized growth mechanisms including laser ablation, capillary flow of laser-induced melt layers, and redeposition of ablated material. Surface features induced by one laser pulse affect the absorption of light from subsequent pulses, resulting in feedback during formation. The resulting microscale surface structures are overlaid with a thick layer of nanoparticles produced and redeposited during the ablation process. The size and shape of the FLSP generated surface features are controlled through laser parameters including pulse fluence and the number of laser pulses incident per area on the sample. A more detailed description of the dynamics of the FLSP technique can be found in previous publications [18–20,25]. Previous material composition analysis work completed on nickel and stainless steel 304 for features generated through FLSP in open atmosphere revealed oxygen in the nanoparticle layer, which has been attributed to surface oxidation. It should be noted, however, that the study found no foreign materials (materials not native to the substrate) within the bulk of the microscale structures or in the nanoparticle layer [20,25].

The laser used to produce the test sample was a Spectra Physics Spitfire, Ti:Sapphire femtosecond laser system (Figure 1A), which was capable of producing 1 mJ, 80 fs pulses, with a center wavelength of 800 nm. The pulse length and chirp were monitored using a Frequency Resolved Optical Gating (FROG) instrument from Positive Light (Model 8-02). The Gaussian pulses were focused onto the sample surface using a 125 mm focal length plano-convex lens. The position of the sample with respect to the laser focal volume was controlled using computer-guided Melles Griot nanomotion translation stages with 3 axes of motion. The laser power was controlled using a half waveplate and a polarizer. All surface processing was completed in open atmosphere. In the present study, the target sample was processed using a peak pulse fluence of 2.20 J/cm^2 and translated at a speed such that the number of incident pulses per spot was 456.

Prior to processing, test surfaces were fabricated by cutting one square inch pieces of stainless steel 316 and prepared with increasingly fine grit sandpaper and buffing compound until a mirror-finish had been achieved. Surfaces were then cleaned via a multistep process. Samples were rinsed with acetone followed by a 20 minute ultrasonic bath in distilled water. Samples were then dried with compressed air and cleaned with a frozen CO_2 sprayer. Finally, the samples were ultrasonically cleaned for 20 minutes in distilled water and dried with compressed air. After FLSP, samples were sputtered with 200 nm cerium oxide and subsequently characterized via, X-Ray Diffraction (XRD), Scanning Electron Microscopy (SEM), and contact angle. XRD was performed using a PANalytical Empyrean with Cu K_α radiation. SEM was performed in a FEI Helios 660 operating at 20kV with an EDAX SDD Octane super EDS detector. The samples were then heated via a stainless steel heating block controlled by a programmable Ramé-Hart temperature controller with a resolution of 0.1˚C (Figure 1B). A thermocouple was embedded just below the surface of the block on which the samples were placed in order to provide feedback to the temperature controller. Samples were annealed by temperatures increasing by 20˚C. After each heating cycle the sample was allowed to cool to room temperature and monitored via contact angle and XRD.

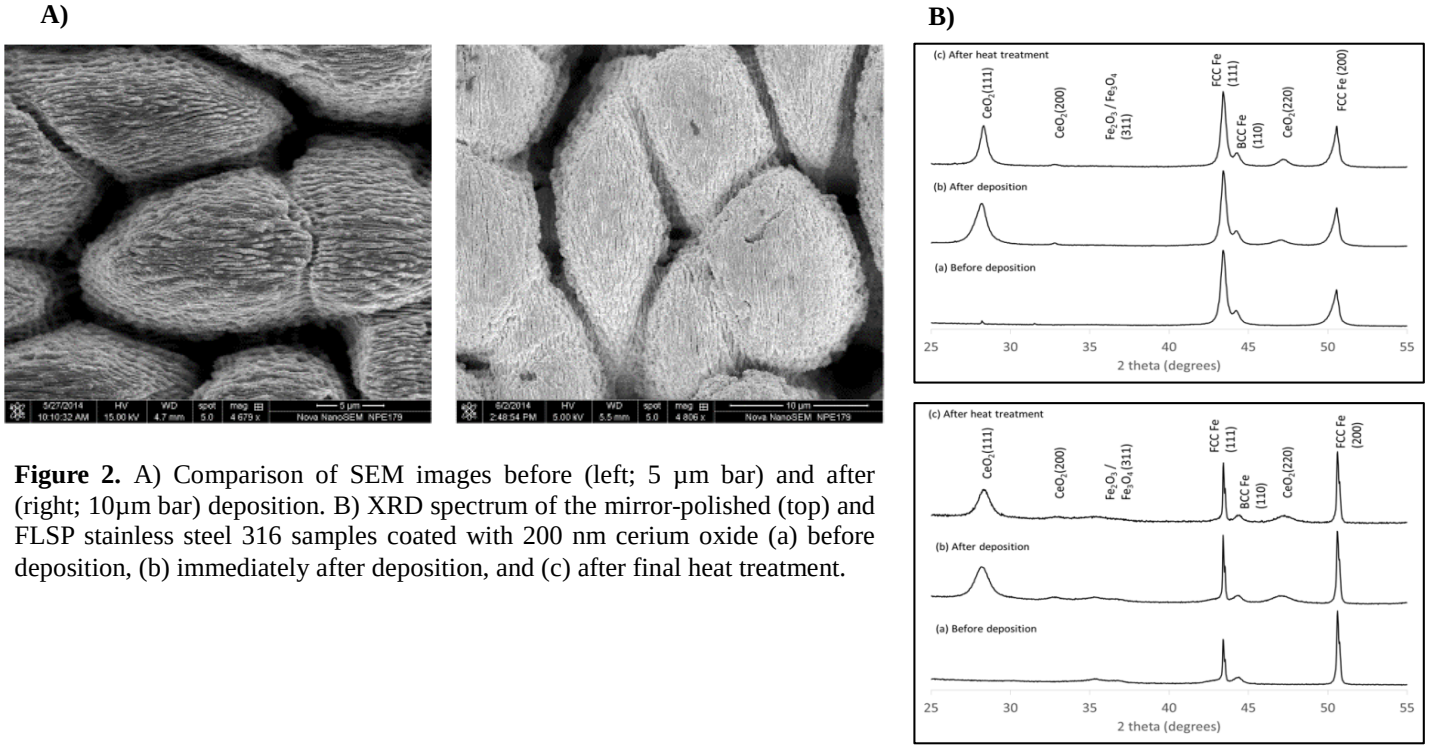

Figure 2. A) Comparison of SEM images before (left; 5 µm bar) and after (right; 10µm bar) deposition. B) XRD spectrum of the mirror-polished (top) and FLSP stainless steel 316 samples coated with 200 nm cerium oxide (a) before deposition, (b) immediately after deposition, and (c) after final heat treatment.

Figure 2A shows SEM images of the FLSP surface before and after ceria deposition. After deposition, ridges on the microstructures appear to be more rounded and tightly packed. Figure 2B gives XRD results for the polished sample before and after ceria deposition, as well as post heat treatments. The XRD results show there were no phase changes occurring on the surface during heat treatments.

The results of the annealing process on the contact angle of the FLSP and mirror-polished samples can be seen in figure 3A. The initial contact angles were 133˚ and 95˚ for the processed and smooth (mirror-polished) surfaces, respectively. For the FLSP surface, there was a steady increase in hydrophobicity with temperature until approximately 140˚C, at which point there was a rapid decline in the contact angle. The mirror-polished sample showed a similar trend until about 120˚C at which point there was a more gradual decline in the contact angle of the surface. Subsequently, samples were left in laboratory air for one week, over which time hydrophobicity returned to pre-heat-treatment levels. Cleaning the samples with a 20 minute ultrasonic bath in isopropyl alcohol resulted in samples becoming superhydrophilic. It became apparent that REO's are in fact not intrinsically hydrophobic as had been suggested by [15]. Our observations were now in agreement with a study [16] that appeared in the literature while the

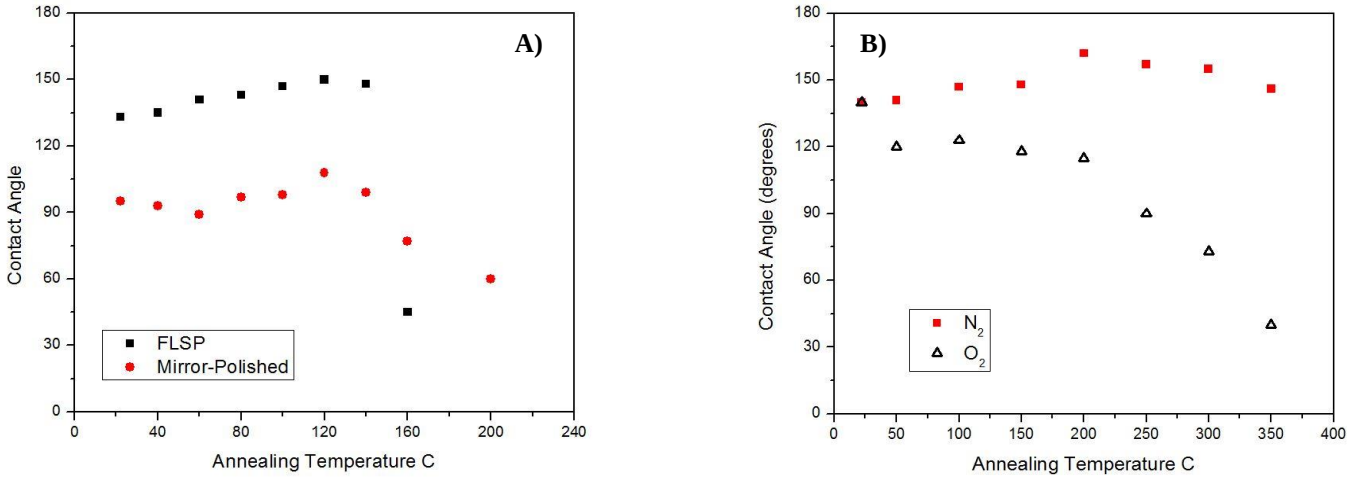

Figure 3. A) Contact angle as a function of annealing temperature in ambient air for FLSP and mirror-polished surfaces sputtered with 200nm of Cerium Oxide. B) Effects of gas composition on contact angle as a function of annealing temperature for an FLSP sample sputtered with 200nm of Cerium Oxide.

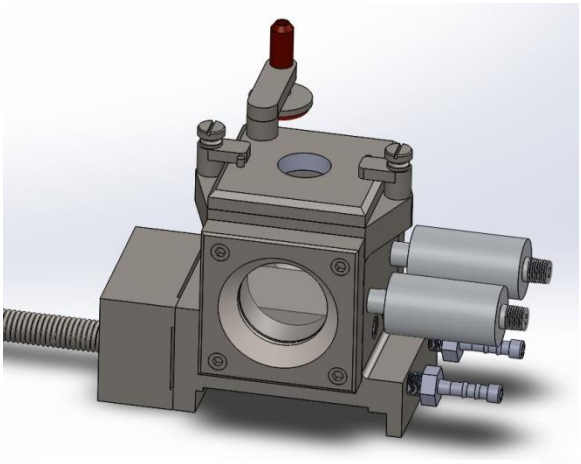

Figure 4. Environmental heating chamber.

present study was conducted: samples which had been stored in laboratory air had adsorbed hydrocarbons, a natural process to reduce surface energy. Heating the samples had subsequently caused the hydrocarbons to be removed from the surface [26,27], rendering the samples hydrophilic. It was interesting to note, however, that prior to loss of hydrocarbons, contact angle was increasing with annealing temperature. This suggests that delamination effects may have assisted in roughening the nanostructure thus promoting Cassie-Baxter wetting. Furthermore, post heat treatment, samples showed contact angles lower than the original values on polished stainless steel further indicating that the surfaces did not regress to their original, pre-deposition state.

Subsequently, the samples were stored in laboratory air and allowed to regain hydrophobicity once again. The FLSP sample was then heated in a nitrogen gas heating environment. In order to isolate atmospheric effects during heating, the sample was heated in a Ramé-Hart environmental chamber (Figure 4). This chamber had a K-type thermocouple embedded just below the surface, and two evenly-spaced cartridge heaters for heating purposes. The chamber was controlled by the previously mentioned Ramé-Hart temperature controller with 0.1˚C resolution. The thermocouple provided feedback to the controller which maintained the desired temperature by varying output. A small sealable hatch in the top could be opened to deposit drops for contact angle measurements. The chamber was equipped with flow nozzles such that the device could function as a purge box.

The FLSP sample then underwent the cyclic heat treatment in the controlled environment up to 350˚C due to experimental setup limitations. During heating and contact angle measurement, the chamber was exposed to a flow of nitrogen gas (99.9% purity, Matheson TRIGAS) so as to displace any ambient contaminants. The hose outlet was held beneath water so as to prevent any backflow. After the annealing in nitrogen was complete, the sample was again placed in the laboratory, allowed to regenerate, and placed back into the chamber to repeat the heat treatments. The sample underwent the same heating process, this time exposed to oxygen gas (99.6%, Matheson TRIGAS). As can be seen from Figure 3B, the FLSP surface retained hydrophobicity throughout the duration of the annealing process when it occurred in inert nitrogen whereas hydrophobicity was lost in an oxygen environment. Roughening of a surface can aid adsorption and thus promote stability due to increased surface area [17] which may help explain why the FLSP surface was able to maintain hydrophobicity even when heated to temperatures above ~260˚C, where hydrogen bonds are thought to degrade [26,27]. However, the fact that different results were observed in an oxygen environment suggests the presence of a chemical reaction on the surface. One possible explanation would be oxidation, as new oxidation could facilitate removal of hydrocarbons from the surface. Additionally, new oxidation layers could grow over surface contaminants, blocking them from interacting with water; however, ceria was deposited in the oxidized state (CeO_2), making this explanation less plausible.

After annealing processes were completed, Thermal Gravimetric Analysis (TGA) was performed in order to determine the temperature at which hydrocarbons will be removed from an FLSP surface. Figure 5 shows the results of the TGA tests; the horizontal axis represents temperature while the vertical axis represents mass change in milligrams. The blue curve represents a clean FLSP sample being heated to 600˚C and then cooled back to room temperature while the gold curve represents an FLSP sample that has been contaminated with hydrocarbons. As can be seen on the figure, there is almost no change in the curve between heating and cooling for the clean surface, while the contaminated surface experienced mass loss between about 165˚C and 275˚C. This temperature range directly corresponds to temperatures reported in the literature at which hydrogen-carbon bonds will break resulting in lost hydrophobicity on organically contaminated surfaces [26,27]. Cooling the originally contaminated surface back to room temperature did not result in any significant mass gain on the sample indicating that the mass loss was a permanent result of lost hydrocarbons. The temperatures over which mass loss

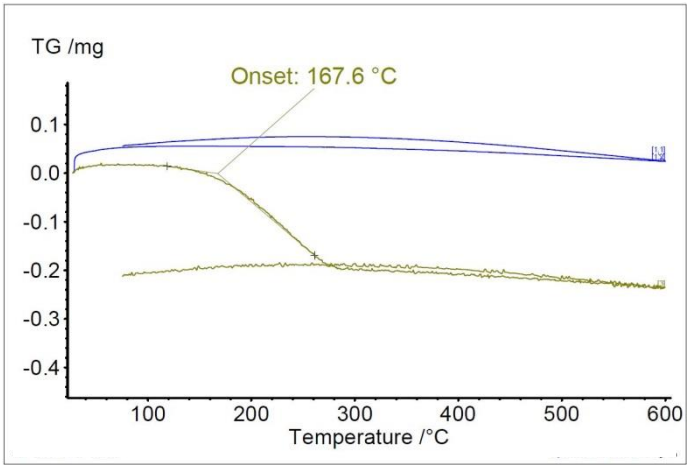

Figure 5. TGA results for a superhydrophilic FLSP sample (blue) and a superhydrophobic FLSP sample (gold).

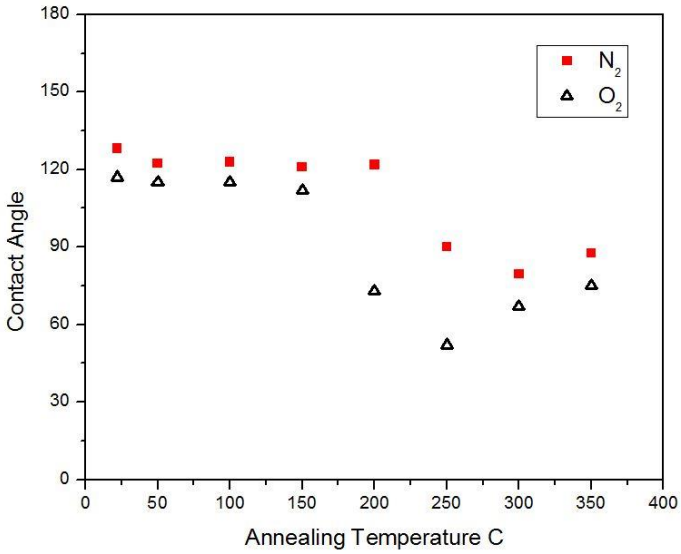

Figure 6. Effects of gas composition on the contact angle of mirror-polished stainless steel 310 sputtered with CeO_2 as a function of annealing temperature.

occurred during TGA are very similar to the temperatures at which the samples shown in figure 3 began to lose hydrophobicity, indicating a direct correlation between surface hydrocarbon content and hydrophobicity.

MIRROR-POLISHED COATED WITH CEO_2

In order to verify the observed atmospheric effects on the thermal stability of REO coatings, two new mirror-polished test surfaces were created in the manner previously described in this paper. After sputtering, the surfaces were placed into a hydrocarbon rich environment to accelerate surface hydrocarbon adsorption. Surfaces were then characterized via EDS prior to any heat treatment. The new test surfaces were heated in the controlled environments used previously on the FLSP surface; one sample was tested in nitrogen the other was tested in oxygen. Figure 6 shows the results of annealing test on the mirror-polished CeO_2 surfaces in nitrogen and oxygen. The initial contact angles for the samples were 128˚ and 117˚ respectively; contact angle values are higher than those reported for flat ceria samples [15,16] as a result of increased hydrocarbon concentrations. The samples began to lose hydrophobicity at 200˚C and 250˚C when heated in oxygen and nitrogen respectively. As can be seen on the graph, atmospheric conditions have similar effects on the annealing temperature dependent contact angle for the smooth and FLSP surface

Table 1. EDS measurements of mirror-polished samples before and after the final heat treatment.

	Sample 1		Sample 2	
	Pre Heating	Post Heating	Pre Heating	Post Heating
Carbon	28 ± 3.3	24.7 ± 1.6	22.0 ± 0.2	21.5 ± 0.3
Oxygen	17.2 ± 3.0	18.1 ± 3.0	22.2 ± 1.0	22.8 ± 0.8
Cerium	3.2 ± 1.0	3.4 ± 1.2	5.0 ± 0.3	5.0 ± 0.4

though the extent of their effects is different. Loss of hydrophobicity in the oxygen environment occurs at a temperature approximately 50˚C below the temperature of hydrophobicity loss in the nitrogen rich environment. The contact angle dependence on annealing temperature however followed a similar trend for both samples. Table 1 shows EDS measurements for the flat ceria samples. Sample 1, heated in nitrogen, showed significant carbon loss as a result of the annealing process, while sample 2, heated in oxygen did not show the same carbon loss. The EDS results for sample 2 did not support our hypothesis on carbon loss; however, it does not reject it either. From the time sample 2 was removed from the heat treatment chamber and placed in the EDS measurement system, carbon adsorption could have occurred. Further work is currently being conducted to understand the fundamental mechanisms at play during the annealing experiments.

Contrary to the suggestion in [15], this study has shown that rare earth oxides are not inherently superhydrophobic, but in fact their superhydrophobic behavior is attributed to the adsorption of hydrocarbons as suggested in [16]. Additionally, thermal stability of ceria surfaces was investigated and found to depend on ambient heating environment. Nearly superhydrophobic surfaces were created by roughening a surface via FLSP and deposition of ceria. Subsequent heating resulted in a decrease in contact angle at similar temperatures to the temperature at which hydrocarbons were shown to be removed from metals during TGA analysis. This reduction in hydrocarbons is found to be the reason for the decrease in contact angle as there was no structural change to the ceria layer and EDS measurements showed a decrease in surface carbon content. It was also noted that sample heated in a nitrogen environment showed improved thermal stability over samples heated in oxygen or ambient air, with nearly superhydrophobic properties persisting through heating to about 380˚C. Further experimentation resulted in the creation of flat ceria samples with contact angles significantly higher than those previously reported, due to increased hydrocarbon concentration on the surface. Subsequent annealing of the flat surfaces resulted in a loss of hydrophobicity over the same temperature range suggested by the FLSP surface and TGA analysis confirming that hydrocarbon adsorption is the underlying mechanism for hydrophobicity in rare earth oxide ceramics.

ACKNOWLEDGMENTS

This work has been supported by a grant through the Nebraska Center for Energy Sciences Research (NCESR) with funds provided by Nebraska Public Power District (NPPD) to the University of Nebraska – Lincoln (UNL) No. 4200000844, a NASA EPSCoR Grant # -NNX13AB17A and by funds from the Department of Mechanical and Materials Engineering and the College of Engineering at UNL, awarded to SN. The authors would like to thank Ethan Davis for creating the model of the environmental heating chamber.

REFERENCES

[1] Enright, R., Miljkovic, N., Alvarado, J. L., Kim, K., and Rose, J. W., 2014, "Dropwise Condensation on Micro- and Nanostructured Surfaces," Nanoscale Microscale Thermophys. Eng., **18**(3), pp. 223–250.

[2] Liu, T., and Kim, C. J., 2014, "Repellent surfaces. Turning a surface superrepellent even to completely wetting liquids," Science., **346**(6213), pp. 1096–1100.

[3] Ems, H., and Ndao, S., 2014, "Fabrication of Inverted Trapezoidal Microstructures for Heat Transfer and Microfluidics Applications," ASME 2014 12th International Conference on Nanochannels, Microchannels, and Minichannels, pp. V001T08A001.

[4] Miljkovic, N., Enright, R., Nam, Y., Lopez, K., Dou, N., Sack, J., and Wang, E. N., 2013, "Jumping-droplet-enhanced condensation on scalable superhydrophobic nanostructured surfaces.," Nano Lett., **13**(1), pp. 179–87.

[5] Ishizaki, T., and Saito, N., 2010, "Rapid formation of a superhydrophobic surface on a magnesium alloy coated with a cerium oxide film by a simple immersion process at room temperature and its chemical stability.," Langmuir, **26**(12), pp. 9749–55.

[6] Manoudis, P. N., Tsakalof, A., Karapanagiotis, I., Zuburtikudis, I., and Panayiotou, C., 2009, "Fabrication of super-hydrophobic surfaces for enhanced stone protection," Surf. Coatings Technol., **203**(10-11), pp. 1322–1328.

[7] Paxson, A. T., Yagüe, J. L., Gleason, K. K., and Varanasi, K. K., 2014, "Stable dropwise condensation for enhancing heat transfer via the initiated chemical vapor deposition (iCVD) of grafted polymer films.," Adv. Mater., **26**(3), pp. 418–23.

[8] Li, Y., Li, L., and Sun, J., 2010, "Bioinspired Self-Healing Superhydrophobic Coatings," Angew. Chemie, **122**(35), pp. 6265–6269.

[9] Wang, H., Xue, Y., Ding, J., Feng, L., Wang, X., and Lin, T., 2011, "Durable, self-healing superhydrophobic and superoleophobic surfaces from fluorinated-decyl polyhedral oligomeric silsesquioxane and hydrolyzed fluorinated alkyl silane.," Angew. Chem. Int. Ed. Engl., **50**(48), pp. 11433–6.

[10] Van der Wal, P., and Steiner, U., 2007, "Super-hydrophobic surfaces made from Teflon," Soft Matter, **3**(4), p. 426.

[11] Guo, Z., Zhou, F., Hao, J., and Liu, W., 2005, "Stable Biomimetic Super-Hydrophobic Engineering Materials," J. Am. Chem. Soc., **157**, pp. 15670–15671.

[12] Erb, A., and Erb, R. A., 1964, "Wettability of Metals under Continuous Condensing Conditions," J. Phys. Chem., **2538**(43), pp. 3–6.

[13] Erb, R., 1973, "Dropwise condensation on gold," Gold Bull., **6**(1), pp. 2–6.

[14] Bartell, F. E., and Cardwell, P. H., 1942, "Reproducible Contact Angles on Reproducible Metal Surfaces. I. Contact Angles of Water against Silver and Gold," J. Am. Chem. Soc., **1863**(2), pp. 494–497.

[15] Azimi, G., Dhiman, R., Kwon, H.-M., Paxson, A. T., and Varanasi, K. K., 2013, "Hydrophobicity of rare-earth oxide ceramics.," Nat. Mater., **12**(4), pp. 315–20.

[16] Preston, D. J., Miljkovic, N., Sack, J., Enright, R., Queeney, J., and Wang, E. N., 2014, "Effect of hydrocarbon adsorption on the wettability of rare earth oxide ceramics," Appl. Phys. Lett., **105**(1), p. 011601.

[17] Kwon, H., 2013, "Tailoring hydrodynamics of non-wetting droplets with nano-engineered surfaces," Ph.D. Thesis, Massachusetts Institute of Technology.

[18] Zuhlke, C. A., Anderson, T. P., and Alexander, D. R., 2013, "Formation of Multiscale Surface Structures on Nickel via Above Surface Growth and Below Surface Growth Mechanisms Using Femtosecond Laser Pulses," Opt. Express, **21**(7), pp. 97–98.

[19] Zuhlke, C. A., Anderson, T. P., and Alexander, D. R., 2013, "Fundamentals of layered nanoparticle covered pyramidal structures formed on nickel during femtosecond laser surface interactions," Appl. Surf. Sci., **283**, pp. 648–653.

[20] Zuhlke, C. A., Anderson, T. P., and Alexander, D. R., 2013, "Comparison of the structural and chemical composition of two unique micro/nanostructures produced by femtosecond laser interactions on nickel," Appl. Phys. Lett., **103**(12), p. 121603.

[21] Vorobyev, A. Y., and Guo, C., 2013, "Direct femtosecond laser surface nano/microstructuring and its applications," Laser Photon. Rev., **7**(3), pp. 385–407.

[22] Nayak, B. K., Gupta, M. C., and Kolasinski, K. W., 2007, "Formation of nano-textured conical microstructures in titanium metal surface by femtosecond laser irradiation," Appl. Phys. A, **90**(3), pp. 399–402.

[23] Tsibidis, G. D., Stratakis, E., Loukakos, P. A., and Fotakis, C., 2013, "Controlled ultrashort-pulse laser-induced ripple formation on semiconductors," Appl. Phys. A, **114**(1), pp. 57–68.

[24] Cassie, B. D., and Baxter, S., 1944, "Wettability of Porous Surfaces," Trans. Faraday Soc., (5), pp. 546–551.

[25] Kruse, C., Anderson, T., Wilson, C., Zuhlke, C., Alexander, D., Gogos, G., and Ndao, S., 2013, "Extraordinary shifts of the Leidenfrost temperature from multiscale micro/nanostructured surfaces.," Langmuir, **29**(31), pp. 9798–806.

[26] Cha, S. C., Her, E. K., Ko, T. J., Kim, S. J., Roh, H., Lee, K.R., Oh, K. H., and Moon, M. W., 2013, "Thermal stability of superhydrophobic, nanostructured surfaces.," J. Colloid Interface Sci., **391**, pp. 152–157.

[27] Tallant, D. R., Parmeter, J. E., Siegal, M. P., and Simpson, R. L., 1995, "The thermal stability of diamond-like carbon," Diam. Relat. Mater., **4**, pp. 191–199.